

Mixed-precision *ab initio* tensor network state methods adapted for NVIDIA Blackwell technology via emulated FP64 arithmetic

Cole Brower,^{1,*} Samuel Rodriguez Bernabeu,^{1,†} Jeff Hammond,^{2,‡} John Gunnels,^{1,§} Sotiris S. Xantheas,^{3,4,¶} Martin Ganahl,^{5,**} Andor Menczer,^{6,7,††} and Örs Legeza^{6,8,9,10,‡‡}

¹NVIDIA, 2788 San Tomas Expressway, Santa Clara, CA 95051

²NVIDIA Helsinki Oy, Porkkalankatu 1, 00180 Helsinki

³Advanced Computing, Mathematics, and Data Division,

Pacific Northwest National Laboratory, Richland, Washington 99354, USA

⁴Department of Chemistry, University of Washington, Seattle, WA 98195, USA

⁵SandboxAQ, Palo Alto, California, USA

⁶Strongly Correlated Systems Lendület Research Group,

Wigner Research Centre for Physics, H-1525, Budapest, Hungary

⁷Eötvös Loránd University, Pázmány Péter Sétány 1/C, 1117 Budapest, Hungary

⁸Dynaflex LTD, Zrínyi u 7, 1028 Budapest, Hungary

⁹Institute for Advanced Study, Technical University of Munich,

Germany, Lichtenbergstrasse 2a, 85748 Garching, Germany

¹⁰Parmenides Stiftung, Hindenburgstr. 15, 82343, Pöcking, Germany

(Dated: October 7, 2025)

We report cutting-edge performance results via mixed-precision spin adapted *ab initio* Density Matrix Renormalization Group (DMRG) electronic structure calculations utilizing the Ozaki scheme for emulating FP64 arithmetic through the use of fixed-point compute resources. By approximating the underlying matrix and tensor algebra with operations on a modest number of fixed-point representatives (“slices”), we demonstrate on smaller benchmark systems and for the active compounds of the FeMoco and cytochrome P450 (CYP) enzymes with complete active space (CAS) sizes of up to 113 electrons in 76 orbitals [CAS(113, 76)] and 63 electrons in 58 orbitals [CAS(63, 58)], respectively, that the chemical accuracy can be reached with mixed-precision arithmetic. We also show that, due to its variational nature, DMRG provides an ideal tool to benchmark accuracy domains, as well as the performance of new hardware developments and related numerical libraries. Detailed numerical error analysis and performance assessment are also presented for subcomponents of the DMRG algebra by systematically interpolating between double- and pseudo-half-precision. Our analysis represents the first quantum chemistry evaluation of FP64 emulation for correlated calculations capable of achieving chemical accuracy and emulation based on fixed-point arithmetic, and it paves the way for the utilization of state-of-the-art Blackwell technology in tree-like tensor network state electronic structure calculations, opening new research directions in materials sciences and beyond.

Introduction: Over the past decade, the rise of deep learning for artificial intelligence has sparked an unprecedented growing demand for computational resources for training and inference of machine learning (ML) models, further fueled by the advent and large-scale deployment of large language models (LLMs). Graphics Processing Units (GPUs) are in many cases the key enabler for ML training and inference, and advances in hardware capabilities often lead to new and more efficient training and inference paradigms [1–5], with NVIDIA’s latest Blackwell hardware generation as a prime example. While AI model training is the prime application of GPUs today, scientists have been investigating how hardware acceler-

ators may be useful in other areas of computational sciences, e.g. scientific computing for materials science and chemistry [6–15]. A key difference between ML model training and scientific computing is arithmetic precision requirements. ML training and inference are typically relatively insensitive to arithmetic precision reduction, a fact that hardware vendors exploit heavily to increase computational throughput for ML training. For example, NVIDIA’s latest Blackwell generation is optimized for reduced precision arithmetic [4, 16, 17], leading to unprecedented computational throughput for ML training and inference. Scientific computing, however, places severe restrictions on arithmetic precision, with double-precision often being mandatory [10, 13]. Here, reduced precision arithmetic may severely impact many linear algebra subroutines, can cause instabilities and may lead to unreliable results. Prominent examples of high-accuracy demands arise in electronic structure calculations [18–34]. Achieving quantitative agreement with experimental results for the electronic structure of a molecule or material requires solving a large, linear system of equations to extremely high accuracy. The typically achievable

* cbrower@nvidia.com

† srodriguezbe@nvidia.com

‡ jeffpapers@nvidia.com

§ jgunnels@nvidia.com

¶ Sotiris.Xantheas@pnnl.gov

** martin.ganahl@sandboxaq.com

†† menczer.andor@wigner.hu

‡‡ legeza.ors@wigner.hu

experimental accuracy in this context is $\sim 1.6\text{mHa}$, also known as the chemical accuracy. In many cases, an accurate solution within this error margin requires prohibitive amounts of memory and computational resources, particularly for chemical compounds containing transition metal elements with many close-lying electronic states [35–40].

A middle ground between these two extremes is the use of mixed-precision arithmetic, i.e. emulated high-precision arithmetic if required, and the use of single- or reduced-precision arithmetic if accuracy and stability permit it. Computational subroutines may flexibly switch between different arithmetic precision levels depending on user-specified speed vs. accuracy tradeoffs. Mixed-precision computing is poised to become increasingly important in the near future, where emulation of floating-point computation can play a major role, allowing systems to flexibly perform not only emulated FP64 operations [41, 42], but a spectrum of FP operations, at precisions not natively supported by the hardware, offering time-to-solution and power efficiency gains [16].

In this context, tensor networks [43–52] are a computational paradigm that is particularly well-suited to benefit from recent advances in hardware design and acceleration [9, 11–14, 53–63]. First risen to fame in the area of computational quantum many-body physics [43–47, 64], use cases have since expanded into quantum chemistry [65–70], machine learning [71–79], computer science [80, 81], and computational fluid dynamics [82–85]. By now, tensor networks have become one of the most promising and powerful approaches to tackle multi-reference systems in an approximate, yet highly accurate, fashion [13, 65, 70, 86–92]. Here, we demonstrate how our highly efficient, hardware-accelerated implementation of the density matrix renormalization group (DMRG) [43] method can be leveraged to perform highly accurate, *ab initio* quantum-chemical electronic structure calculations in mixed-precision arithmetic on NVIDIA’s Blackwell [93] GPU architecture.

Benchmark calculations of our highly-parallelized, GPU-accelerated and $\text{SU}(2)$ -aware implementation of the DMRG algorithm [12, 13, 61–63, 94] are presented on an NVIDIA DGX B200 GPU supercomputer [4] via emulated FP64 arithmetic [16, 17, 41]. This represents the first quantum chemistry evaluation of FP64 emulation for correlated calculations capable of achieving chemical accuracy and emulation based on fixed-point arithmetic; previously, FP64 emulation was evaluated for traditional mean-field (DFT) methods using FP16 precision [95]. Our work forms a major milestone in validating this novel approach in electronic structure calculations and also paves the way for applications via state-of-the-art Blackwell technology-based hardware architectures [4].

Theory of TNS/DMRG regarding error analysis: The DMRG is a variational optimization method for finding the ground state of a model Hamiltonian H over the space of so-called matrix product states (MPS) ansatz wave functions [51]. Given the description of a quan-

tum chemical system [65] in terms of N spinful orbitals $|i_n\rangle = \{|0\rangle, |\uparrow\rangle, |\downarrow\rangle, |\uparrow\downarrow\rangle\}$, its quantum mechanical wave function can be written as

$$|\Psi_{MPS}\rangle = \sum_{\{i_k\}} \sum_{\{\alpha_p\}} [A_1]_{1\alpha_1}^{i_1} [A_2]_{\alpha_1\alpha_2}^{i_2} \cdots [A_N]_{\alpha_{N-1}1}^{i_N} |i_1 \cdots i_N\rangle \quad (1)$$

where $A_{\alpha_{n-1}\alpha_n}^{i_n}$ are order-3 tensors of dimension $(D_{n-1}, 4, D_n)$ except for the first and the last orbitals where order-2 tensors appear. The numerical accuracy of the ansatz is determined by the ranks of the matrices, D , also known as the bond dimension, with higher ranks corresponding to higher accuracy. The exact solution is recovered at $D_n \sim 4^n$ for $1 \leq n \leq N/2$ ($D_n \sim 4^{N-n}$ for $N/2 \leq n \leq N$). In practice, the full ranks are truncated to achieve an approximate solution. The memory and compute requirements scale as $O(N^2 D^2)$ and $O(N^4 D^3)$, respectively. In this work, bond dimensions, D , are reported as $\text{SU}(2)$ multiplets [12, 96, 97]. The DMRG method performs sequential updates one tensor at a time, while keeping all other tensors fixed, such that the expected energy $\langle \Psi_{MPS} | H | \Psi_{MPS} \rangle$ is iteratively lowered.

The first key subroutine is simply binary tensor contraction via matrix multiplications, which is the basic workhorse for any tensor network algorithm. The second subroutine carries out the update for tensor $[A_n]_{\alpha_{n-1}\alpha_n}^{i_n}$. The update is obtained from an iterative diagonalization of an effective Hamiltonian matrix in a truncated Hilbert space of dimension proportional to D^2 , using a Krylov-based eigensolver (Davidson or Lánczos method). The accuracy and stability of this solver is typically quite sensitive to arithmetic precision errors. The third subroutine is used to shift the optimization from $[A_n]_{\alpha_{n-1}\alpha_n}^{i_n}$ to $[A_{n+1}]_{\alpha_n\alpha_{n+1}}^{i_{n+1}}$, and employs a singular value decomposition (SVD) on the optimized joined tensor $[A_{(n,n+1),opt}]_{\alpha_{n-1}\alpha_{n+1}}^{i_n i_{n+1}}$ [51]. The accuracy of these three main algorithmic steps influences the overall error of the DMRG algorithm in a complex way. Our implementation allows us to switch between different CPU- and GPU-based implementations for each of these steps, providing us with an ideal framework to test numerical libraries that implement these operations. The fact that DMRG is a variational method, i.e., that the true ground state energy is strictly approached from above, with an error that is determined by the size of the bond dimension D [48, 98, 99], can be utilized to create a complex test bed to test how arithmetic precision errors affect accuracy and stability of a) the Krylov solver as a function of the residual error ϵ thresholds used therein [51, 100] and b) the SVD truncation. Therefore, from a technical point of view, DMRG provides an ideal tool to validate and benchmark recent hardware developments and numerical libraries by adjusting parameters, even further approximating FP64-precision, so that the final accuracy can be controlled rigorously and performance can be monitored for a broad range of error margins.

Theory of emulated FP64 arithmetic: In the follow-

ing we provide a short description of the key ideas of our FP64 emulation strategy, and refer the reader to the literature for more details [41, 42]. Considering the multiplication of two matrices $\mathbf{C} = \mathbf{A}\mathbf{B}$, the key strategy is as follows: 1) convert floating point values in the matrices to a fixed-point format with exponents shared across each row of \mathbf{A} and each column of \mathbf{B} , 2) decompose the matrices \mathbf{A}, \mathbf{B} into "slices" $\mathbf{A}^i, \mathbf{B}^j$, $i, j \in \{1, \dots, S\}$ of lower precision, 3) perform matrix multiplications in lower precision for all pairs (i, j) independently, and 4) accumulate the products at high precision into the final result $\mathbf{C} = \sum_{ij} \mathbf{A}^i \mathbf{B}^j$. The decomposition into lower-precision matrices can be done in several different ways, as explained in e.g. [42], but all approaches follow similar strategies. For example, the multiplication of two fixed-point numbers, using seven INT8 slices (to hold 63 mantissa bits) to represent each requires 49 (7x7) element-wise multiply-adds (aggregated using a higher precision data type, e.g. INT32). Further efficiencies can be gained by e.g. ignoring the less significant results in the lower-triangular portion of the 7x7 grid above. After the results are aggregated, the individual contributions are converted back into FP64.

Numerical procedure: Our numerical analysis will be presented for various strongly-correlated molecules and chemical clusters, i.e., multi-reference problems. DMRG simulations have been performed on GPU accelerated NVIDIA DGX H100 and DGX B200 single nodes using both traditional FP64 double-precision as well as emulated FP64 arithmetic. The simple formula that connects number of slices, S , to mantissa bit counts is $S = \text{ceil}(\text{div}(\text{mantissabits} + 1, 8))$, which gives mantissa bit setting 15, 23, 31, 39, 47, 55 when approximating double-precision in emulated mode for $S = 2, 3, 4, 5, 6, 7$. The +1 term accounts for the sign bit.

NVIDIA's pre-release cuBLAS library offers various interfaces to test and use emulation with environment variables or corresponding APIs. These environment variables enable/disable emulation, specify the number of mantissa bits or allow the system to dynamically determine this value, and enable eager/performant emulation strategies. With NVIDIA's pre-release cuBLAS library, when no environment variables are set, one will still see native FP64. When emulation is enabled but no mantissa bit count is set, the library determines how many extra bits are needed to maintain the accuracy of native FP64. While emulation is powerful for compute-bound matrix-multiplications, it is often slower for memory-bound matrix multiplications. Eager mode attempts to use emulation irrespective of the performance characteristics of the matrix multiplication problem, whereas performant mode enables a layer of heuristics to choose to use emulation when it would provide a performance advantage. In order to study the numerical properties of mixed precision floating point emulation in DMRG we have used eager mode and set $\varepsilon = 10^{-5}$ in the rest of the paper unless otherwise specified. Moreover, this pre-release library, via performant mode, the default, has an early version of

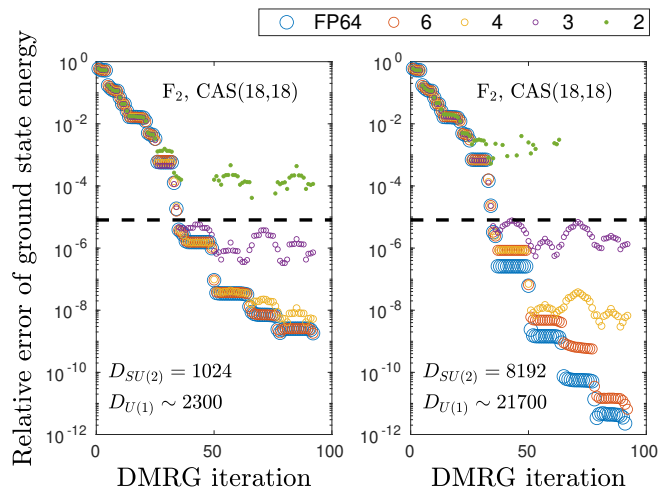


FIG. 1. Relative error of the ground state energy as a function of DMRG iteration steps for the F_2 molecule in a CAS(18,18) model space using $D_{SU(2)} = 1024$ (left panel) and $D_{SU(2)} = 8192$ (right panel) $SU(2)$ multiplets for the non-emulated native FP64 limit and for various number of INT8 slices, $S \in \{6, 4, 3, 2\}$ obtained on a DGX B200 system. The dashed line stands for the relative error of chemical accuracy.

the heuristics that invoke emulation only when it makes sense to do so from a performance perspective. A subsequent publication will include a performance study using an improved cuBLAS library and performant mode. Finally, we remark that results were obtained using a pre-release cuBLAS binary and the data is subject to change upon official release of the library.

Numerical benchmark: The first problem we consider is the F_2 molecule on a CAS(18,18) model space [99], for which the exact full-CI reference energy is also available from exact diagonalization in FP64 precision. In this work all energies will be given in Hartrees (a.u.). In Fig. 1 we show the relative error of the ground state energy as a function of DMRG iteration steps using $D_{SU(2)} = 1024$ (left panel) and $D_{SU(2)} = 8192$ (right panel) $SU(2)$ multiplets for the non-emulated FP64 limit and for various number of INT8 slices, $S \in \{6, 4, 3, 2\}$. We observe for both bond dimensions, D , that the FP64 reference limit is reproduced at $S = 6$ slices, and a systematically increasing relative error with decreasing values of S . We note that $S = 3$ slices are just sufficient to reach chemical accuracy for this system, but in general $S > 3$ is required to obtain more reliable accuracy. Note that we only observe the expected increase in accuracy with increasing D for $S \geq 4$. For $S = 2$, i.e. half-like precision, we observe an error significantly above chemical accuracy, unstable DMRG iterations, and violations of the variational principle (i.e. energies below the exact solution, not shown in Fig. 1).

In Fig.2 we repeat the same analysis for the more challenging case of the nitrogen dimer in the cc-pVDZ basis at equilibrium bond length, $r = 2.118a_0$, and

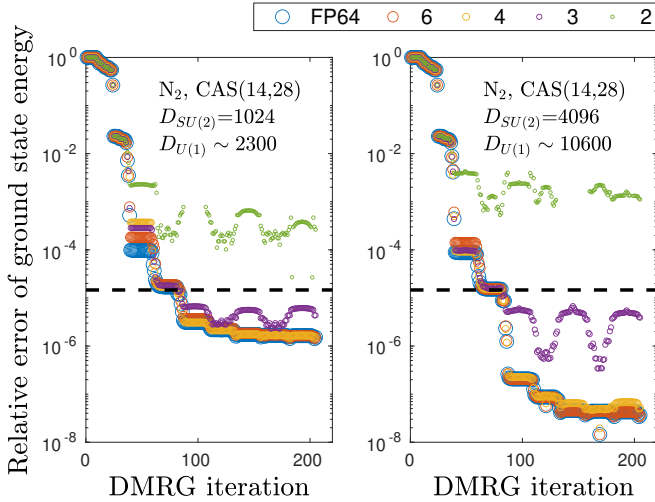


FIG. 2. Similar to Fig. 1 but for the nitrogen dimer at its equilibrium geometry in a CAS(14,28) model space using $D_{SU(2)} = 1024$ (left panel) and $D_{SU(2)} = 4096$ (right panel) $SU(2)$ multiplets obtained on a DGX B200 system.

CAS(14,28), which has been subject of several DMRG benchmark calculations [12, 101–105]. We find similar convergence profiles as summarized in Fig. 2. The reference energy was determined through a highly accurate coupled-cluster, CCSDTQPH calculation [102] and validated by large-scale DMRG simulations up to six decimal digits [12, 102]. For both $D_{SU(2)} = 1024$ and $D_{SU(2)} = 4096$ (left and right panel, respectively) all emulated FP64 energies with $S \geq 3$ converged and reproduced the reference FP64 DMRG data within chemical accuracy, while calculations for $S = 2$ again show poor accuracy, convergence issues, and non-variational energies. Note that the expected increase in accuracy with increasing bond dimension is reproduced only at $S = 4, 6$ slices. In order to study how the eigenvalue spectrum affects numerical stability, we have repeated the same analysis, but for stretched geometries, i.e. for bond distances $r = 3.600a_0$ and $4.200a_0$, where the multi-reference character is becoming more pronounced [103–105]. In general, we again obtain very similar and stable convergence profiles up to the error margins discussed above for $S > 2$, and unstable simulations for $S = 2$.

Next, we targeted a very complex chemical system, the cytochrome P450 (CYP) enzymes, using a CAS(63,58) model space introduced recently by the Google Research team [106]. This system has also been in the focus of our research, demonstrating previously that our hybrid CPU-GPU DMRG code can reach 0.25 PFLOPS performance on a single DGX H100 node [13]. Therefore, highly accurate DMRG reference data are available for the different spin states. In Fig. 3 we present the obtained convergence profiles for the spin-1/2 doublet ground state with $D_{SU(2)} = 2048$, using both native FP64 and $S \in \{4, 6\}$ slices (left panel), while the absolute error with respect to the native FP64 simulation is

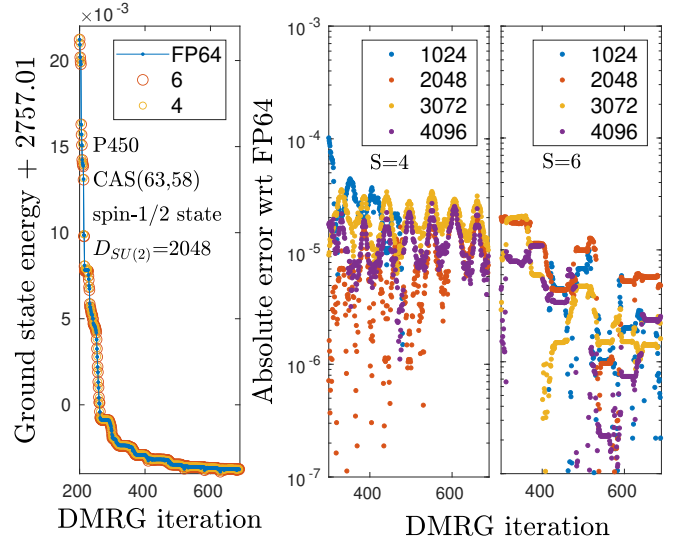


FIG. 3. Shifted ground state energy for the spin-1/2 doublet state of the cytochrome P450 (CYP) enzymes with CAS(63,58) model space as a function of DMRG iteration using $D_{SU(2)} = 2048$ $SU(2)$ multiplets and $S \in \{4, 6\}$ slices (left panel) and the absolute error measured with respect to the native FP64 data sets for $S = 4$ (central panel) and $S = 6$ (right panel) slices for various D values obtained on a DGX B200 system.

presented in the central and right panels for various bond dimensions. It is clearly visible that stable convergence can be reached with $S \geq 4$ number of slices. The absolute error for $S = 6$ upon convergence is already in the range of 10^{-5} for $D_{SU(2)} = 1024$, which drops further down to $10^{-6} - 10^{-7}$ with increasing bond dimension. Similar results have been obtained for the spin-3/2 and spin-5/2 excited states. For $S = 4$ a slightly larger error is obtained, while for $S = 3$ the absolute error was even larger than the chemical accuracy for all $D \geq 1024$ values. Therefore, using $S \in \{4, 6\}$ slices we managed to reproduce our earlier results [13] for the spin gaps within microHartree accuracy via mixed-precision arithmetic on state-of-the-art Blackwell hardware.

Finally, for the FeMoco on CAS(54,54) [107, 108] and CAS(113,76) model spaces [12, 14, 57, 109] we have found similar error profiles using $S \in \{4, 6\}$ slices as discussed in Fig. 3. In practice, the optimal number of slices are set automatically by default (performant mode) based on the most recent version of the pre-release cuBLAS library, which returned even slightly more accurate energy values. This let us conclude again that in electronic structure calculations, utilization of a limited number of slices $S \in \{4, 6\}$ is adequate to reach chemical accuracy.

Numerical stability: To gather more details about the convergence of DMRG, its main algorithmic parts can be analyzed independently by switching between a CPU-based implementation or a CUDA version using double-precision or emulated FP64. First, we found that the

number of Lánczos iteration steps for the diagonalization of the effective Hamiltonian (for more detailed terminology see Refs. [12, 61, 69, 110]) is almost the same for $S \geq 3$ slices, in agreement with FP64 reference data. Consequently, the Lánczos method is not sensitive to the enforced approximations used via the DGEMM operations [111] and a stable convergence can be obtained. In contrast to this, for $S = 2$ slices non-variational solutions have been returned for several DMRG iteration steps. This led to a complete failure of DMRG as shown in Figs. 1 and 2. Reducing the residual error ε to $10^{-4}, \dots, 10^{-2}$, the number of non-variational eigenvalues, however, disappeared leading to an oscillating curve in relative energy in the range of 10^{-4} as in Fig. 1, but without “missing” data points (for more details, see Fig. 9 in the Supporting Information). We remark that we found the Davidson method less stable using emulated FP64 arithmetic with a reduced slice count, reflected by the slightly increased number of iterations during the iterative diagonalization procedure.

Next, we analyzed the effect of employing a CPU, via native FP64, or GPU, via emulated FP64, implementation of the network contraction, i.e. renormalization step, which is also based on DGEMM operations. In general, we obtained similar and stable convergence profiles for $S \geq 3$ slices regardless of whether we used a CPU or GPU version. Finally, we studied the effect of the eigenvalue solver offered by cuSOLVER to diagonalize the reduced density matrix and truncate Schmidt-spectrum accordingly. By employing the CPU-based Intel MKL LAPACK function (*LAPACKE_dsyevd*) via native FP64 or the GPU implementation (*cusolverDnXsyevd*) and carrying out the related linear algebra via reduced-precision emulated FP64-like arithmetic we have found significant effects on the convergence of the DMRG method for small $S \in \{2, 3\}$ slices, and the error accumulated via SVD determines the overall convergence (for more details see Figs. 8 and 10 in the Supporting Information). A more rigorous error analysis, also employing the dynamic block state selection (DBSS) approach [99, 112], will be part of a subsequent publication.

Performance assessment: In Fig. 4 we present the accumulated wall time in minutes for the diagonalization of the effective Hamiltonian for simulations discussed in Fig. 1. It is evident that when eager mode is enforced, i.e., when almost all matrices employ emulation, the wall time increases significantly for $S \geq 3$ slices compared to the native FP64 limit. Without using eager mode, however, the FP64 profile is basically recovered and even a slightly lower wall time is found for $S \in \{4, 6\}$ for the larger $D = 8192$ simulations. For completeness, we also present performance assessment in Fig. 5 by comparing maximum performance measured in TFLOPS via the diagonalization of the effective Hamilton operator for the native FP64 limit on DGX H100 and DGX B200 systems. For smaller D values a significant increase in performance becomes apparent on the Blackwell node, while after a crossover, a 10-15% decrease in performance is

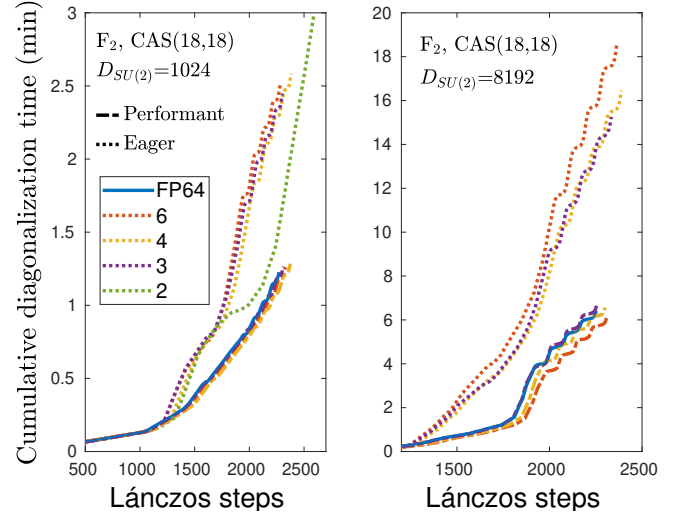


FIG. 4. Cumulative diagonalization time in minutes as a function of Lánczos steps for simulations discussed in Fig. 1 obtained on a DGX B200 system. In practice the performant mode (non-Eager mode), where the system decides when it is faster to run emulation, is used.

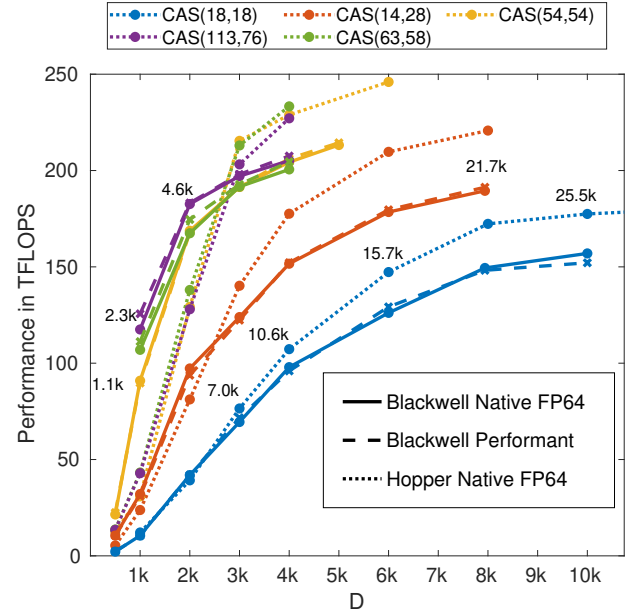


FIG. 5. Benchmark results obtained via the SU(2) spin-adapted single node hybrid CPU plus multi-GPU DMRG calculations for the F_2 molecule on a CAS(18,18) orbital space [99], the N_2 molecule on a CAS(14,28) space [102], FeMoco on CAS(54,54) [107] and CAS(113,76) [109] spaces, and P450 on CAS(63,58) [106]. The solid lines correspond to calculations performed on a DGX B200 system via native FP64 precision, while dashed lines correspond to emulated performant mode. As a reference, the dotted lines trace the results obtained on a DGX H100 system [13]. Numbers indicate the corresponding $U(1)$ bond dimension values, which are the same for the dotted, dashed, and the solid lines.

observed for larger D values. On the DGX B200 system similar profiles have also been obtained via the emulated (performant) mode which for larger D values and larger system sizes, N , slightly improve performance and efficiency. Therefore, we expect algorithms and implementations to improve and make a bigger impact on DMRG performance in the future. A subsequent publication will include a more detailed performance analysis using an improved cuBLAS library and performant mode.

We remark that our hybrid CPU-multiGPU DMRG implementation can exploit almost the full power of the Blackwell system for large bond dimensions and system sizes, reflected by the fact that 90-95% of the Thermal Design Power (TDP) was utilized, i.e. 900-950 Watts for each GPU card. Moreover, DGX B200 is very beneficial to fulfill the large memory demands of *ab initio* DMRG, as it offers a total of 1.44 TB of GPU memory.

Conclusion: We presented numerical analysis and benchmark calculations of recent developments based on the Ozaki scheme for emulating FP64 arithmetic through the use of fixed-point compute resources by employing the massively parallel spin-adapted *ab initio* density matrix renormalization group (DMRG) method on selected strongly correlated chemical systems. By adjusting matrix ranks (bond dimensions) and system sizes, we performed a detailed error and performance analysis by approximating FP64 arithmetic with lower precision fixed-point elements (referred to as “slices”) and demonstrated that chemical accuracy can be reached via mixed-precision arithmetic using limited number of slices. How-

ever, for the half-like precision limit (two slices) the obtained ground state energy values can become unphysical and fall below the exact reference energy, showing that such crude approximation is not acceptable. Benchmark profiles obtained on the DGX B200 system showed only a slight decrease in performance rate compared to that of a DGX H100 node, which is expected to be compensated via the improved cuBLAS library and performant mode in the near future. Finally, utilization of the presented mixed-precision arithmetic for orbital optimization via the GPU-aware DMRG-SCF framework [113] is straightforward. Taken together, these highlight the efficient utilization of state-of-the-art Blackwell technology in tree-like tensor network state electronic structure calculations, opening new research directions in materials sciences and beyond.

Acknowledgments: This work has been supported by the Hungarian National Research, Development and Innovation Office (NKFIH) through Grant Nos. K134983 and TKP2021-NVA-04, and by the Center for Scalable and Predictive methods for Excitation and Correlated phenomena (SPEC), funded as part of the Computational Chemical Sciences, FWP 70942, by the U.S. Department of Energy (DOE), Office of Science, Office of Basic Energy Sciences, Division of Chemical Sciences, Geosciences, and Biosciences at Pacific Northwest National Laboratory. Ö.L. acknowledges financial support by the Hans Fischer Senior Fellowship programme funded by the Technical University of Munich – Institute for Advanced Study.

-
- [1] NVIDIA, NVIDIA DGX GH200. <https://resources.nvidia.com/en-us-dgx-systems/nvidia-dgx-gh200-datasheet-web-us>, <https://resources.nvidia.com/en-us-dgx-systems/nvidia-dgx-gh200-datasheet-web-us>.
 - [2] AMD, AMD INSTINCT MI300A APU. <https://www.amd.com/content/dam/amd/en/documents/instinct-tech-docs/data-sheets/amd-instinct-mi300a-data-sheet.pdf>, <https://www.amd.com/content/dam/amd/en/documents/instinct-tech-docs/data-sheets/amd-instinct-mi300a-data-sheet.pdf>.
 - [3] Jouppi, N. P.; Yoon, D. H.; Kurian, G.; Li, S.; Patil, N.; Laudon, J.; Young, C.; Patterson, D. A domain-specific supercomputer for training deep neural networks. *Commun. ACM* **2020**, *63*, 67–78.
 - [4] NVIDIA, NVIDIA Blackwell Architecture Technical Brief. <https://resources.nvidia.com/en-us-blackwell-architecture>, <https://resources.nvidia.com/en-us-blackwell-architecture>.
 - [5] Groq, Why AI Requires a New Chip Architecture. <https://groq.com/why-ai-requires-a-new-chip-architecture/>, <https://groq.com/why-ai-requires-a-new-chip-architecture/>.
 - [6] Seritan, S.; Bannwarth, C.; Fales, B. S.; Hohenstein, E. G.; Isborn, C. M.; Kokkila-Schumacher, S. I. L.; Li, X.; Liu, F.; Luehr, N.; Snyder Jr., J. W.; Song, C.; Titov, A. V.; Ufimtsev, I. S.; Wang, L.-P.; Martínez, T. J. TeraChem: A graphical processing unit-accelerated electronic structure package for large-scale *ab initio* molecular dynamics. *WIREs Computational Molecular Science* **2021**, *11*, e1494.
 - [7] Kresse, G.; Hafner, J. *Ab initio* molecular dynamics for liquid metals. *Phys. Rev. B* **1993**, *47*, 558–561.
 - [8] Giannozzi, P. et al. Advanced capabilities for materials modelling with QUANTUM ESPRESSO. *Journal of Physics: Condensed Matter* **2017**, *29*, 465901.
 - [9] Ganahl, M.; Milsted, A.; Leichenauer, S.; Hidary, J.; Vidal, G. TensorNetwork on TensorFlow: Entanglement Renormalization for quantum critical lattice models. *arxiv:1906.1203* **2019**,
 - [10] Pederson, R.; Kozłowski, J.; Song, R.; Beall, J.; Ganahl, M.; Hauru, M.; Lewis, A. G. M.; Yao, Y.; Mallick, S. B.; Blum, V.; Vidal, G. Large Scale Quantum Chemistry with Tensor Processing Units. *Journal of Chemical Theory and Computation* **2023**, *19*, 25–32, PMID: 36508260.
 - [11] Ganahl, M.; Beall, J.; Hauru, M.; Lewis, A. G.; Wojno, T.; Yoo, J. H.; Zou, Y.; Vidal, G. Density Matrix Renormalization Group with Tensor Processing Units. *PRX Quantum* **2023**, *4*, 010317.
 - [12] Menczer, A.; Legeza, O. Tensor Network State Algorithms on AI Accelerators. *Journal of Chemical Theory and Computation* **2024**, *20*, 8897–8910.
 - [13] Menczer, A.; van Damme, M.; Rask, A.; Hunting-

- ton, L.; Hammond, J.; Xantheas, S. S.; Ganahl, M.; Legeza, O. Parallel implementation of the Density Matrix Renormalization Group method achieving a quarter petaFLOPS performance on a single DGX-H100 GPU node. *Journal of Chemical Theory and Computation* **2024**, *20*, 8397–8404.
- [14] Xiang, C.; Jia, W.; Fang, W.-H.; Li, Z. A distributed multi-GPU ab initio density matrix renormalization group algorithm with applications to the P-cluster of nitrogenase. *Journal of Chemical Theory and Computation* **2024**, *20*, 775–786.
- [15] Agarawal, V.; Khurana, R.; Liu, C.; Hermes, M. R.; Knight, C.; Gagliardi, L. Enabling Multireference Calculations on Multimetallic Systems with Graphic Processing Units. *Journal of Chemical Theory and Computation* **2025**, *21*, 7378–7393.
- [16] Dongarra, J.; Gunnels, J.; Bayraktar, H.; Haidar, A.; Ernst, D. Hardware Trends Impacting Floating-Point Computations In Scientific Applications. 2024; <https://arxiv.org/abs/2411.12090>.
- [17] Yokota, R. NVIDIA, TOP500 BoF: Algorithmic Innovation for Scaling the Power Wall in the AI Era. 2024.
- [18] Swart, M.; Gruden, M. Spinning around in Transition-Metal Chemistry. *Accounts of Chemical Research* **2016**, *49*, 2690–2697, PMID: 27993008.
- [19] Khedkar, A.; Roemelt, M. Modern multireference methods and their application in transition metal chemistry. *Phys. Chem. Chem. Phys.* **2021**, *23*, 17097–17112.
- [20] Feldt, M.; Phung, Q. M. Ab Initio Methods in First-Row Transition Metal Chemistry. *European Journal of Inorganic Chemistry* **2022**, *2022*, e202200014.
- [21] Pantazis, D.; Orio, M.; Petrenko, T.; Zein, S.; Bill, E.; Lubitz, W.; Messinger, J.; Neese, F. A New Quantum Chemical Approach to the Magnetic Properties of Oligonuclear Transition-Metal Complexes: Application to a Model for the Tetranuclear Manganese Cluster of Photosystem II. *Chemistry – A European Journal* **2009**, *15*, 5108–5123.
- [22] Sharma, S.; Sivalingham, K.; Neese, F.; Chan, G. K.-L. Low-energy spectrum of iron–sulfur clusters directly from many-particle quantum mechanics. *Nature Chemistry* **2014**, *6*, 927–933.
- [23] Vinyard, D. J.; Brudvig, G. W. Progress Toward a Molecular Mechanism of Water Oxidation in Photosystem II. *Annual Review of Physical Chemistry* **2017**, *68*, 101–116, PMID: 28226223.
- [24] Lubitz, W.; Chrysina, M.; Cox, N. Water oxidation in photosystem II. *Photosynthesis Research* **2019**, *142*, 105–125.
- [25] Kerridge, A. *Computational Methods in Lanthanide and Actinide Chemistry*; John Wiley & Sons, Ltd, 2015; Chapter 5, pp 121–146.
- [26] Spivak, M.; Vogiatzis, K. D.; Cramer, C. J.; Graaf, C. d.; Gagliardi, L. Quantum Chemical Characterization of Single Molecule Magnets Based on Uranium. *The Journal of Physical Chemistry A* **2017**, *121*, 1726–1733, PMID: 28128563.
- [27] Gaggioli, C. A.; Gagliardi, L. Theoretical Investigation of Plutonium-Based Single-Molecule Magnets. *Inorganic Chemistry* **2018**, *57*, 8098–8105.
- [28] Saue, T. Relativistic Hamiltonians for Chemistry: A Primer. *ChemPhysChem* **2011**, *12*, 3077–3094.
- [29] Pyykkö, P. Relativistic effects in chemistry: more common than you thought. *Annual review of physical chemistry* **2012**, *63*, 45–64.
- [30] Reiher, M.; Wolf, A. *Relativistic Quantum Chemistry*; John Wiley & Sons, Ltd, 2014; Chapter 14, pp 527–566.
- [31] Tecmer, P.; Boguslawski, K.; Kedziera, D. In *Handbook of Computational Chemistry*; Leszczynski, J., Ed.; Springer Netherlands: Dordrecht, 2016; pp 1–43.
- [32] Liu, W. Essentials of relativistic quantum chemistry. *The Journal of Chemical Physics* **2020**, *152*, 180901.
- [33] Becke, A. D. Density functionals for static, dynamical, and strong correlation. *The Journal of Chemical Physics* **2013**, *138*, 074109.
- [34] Benavides-Riveros, C. L.; Lathiotakis, N. N.; Marques, M. A. L. Towards a formal definition of static and dynamic electronic correlations. *Phys. Chem. Chem. Phys.* **2017**, *19*, 12655–12664.
- [35] Kinoshita, T.; Hino, O.; Bartlett, R. J. Coupled-cluster method tailored by configuration interaction. *The Journal of Chemical Physics* **2005**, *123*, 074106.
- [36] Bartlett, R. J.; Musiał, M. Coupled-cluster theory in quantum chemistry. *Rev. Mod. Phys.* **2007**, *79*, 291–352.
- [37] Lischka, H.; Nachtigallova, D.; Aquino, A. J. A.; Szalay, P. G.; Plasser, F.; Machado, F. B. C.; Barbatti, M. Multireference Approaches for Excited States of Molecules. *Chemical Reviews* **2018**, *118*, 7293–7361.
- [38] Evangelista, F. A. Perspective: Multireference coupled cluster theories of dynamical electron correlation. *The Journal of Chemical Physics* **2018**, *149*, 030901.
- [39] Pulay, P. A perspective on the CASPT2 method. *International Journal of Quantum Chemistry* **2011**, *111*, 3273–3279.
- [40] Szalay, P. G.; Muller, T.; Gidofalvi, G.; Lischka, H.; Shepard, R. Multiconfiguration Self-Consistent Field and Multireference Configuration Interaction Methods and Applications. *Chemical Reviews* **2012**, *112*, 108–181.
- [41] Ootomo, H.; Ozaki, K.; Yokota, R. DGEMM on integer matrix multiplication unit. *The International Journal of High Performance Computing Applications* **2024**, *38*, 297–313.
- [42] Uchino, Y.; Ozaki, K.; Imamura, T. Performance enhancement of the Ozaki Scheme on integer matrix multiplication unit. *The International Journal of High Performance Computing Applications* **2025**, *39*, 462–476.
- [43] White, S. R. Density-matrix algorithms for quantum renormalization groups. *Phys. Rev. B* **1993**, *48*, 10345–10356.
- [44] White, S. R. Spin Gaps in a Frustrated Heisenberg Model for CaV_4O_9 . *Phys. Rev. Lett.* **1996**, *77*, 3633–3636.
- [45] Fannes, M.; Nachtergaele, B.; Werner, R. F. Exact Antiferromagnetic Ground States of Quantum Spin Chains. *EPL (Europhysics Letters)* **1989**, *10*, 633.
- [46] Östlund, S.; Rommer, S. Thermodynamic Limit of Density Matrix Renormalization. *Phys. Rev. Lett.* **1995**, *75*, 3537–3540.
- [47] Rommer, S.; Östlund, S. Class of ansatz wave functions for one-dimensional spin systems and their relation to the density matrix renormalization group. *Phys. Rev. B* **1997**, *55*, 2164–2181.
- [48] Legeza, Ö.; Fáth, G. Accuracy of the density-matrix renormalization-group method. *Phys. Rev. B* **1996**, *53*, 14349–14358.

- [49] Verstraete, F.; Cirac, J. I. Renormalization algorithms for Quantum-Many Body Systems in two and higher dimensions. *arXiv [cond-mat.str-el]* **2004**, 0407066.
- [50] Vidal, G. Entanglement Renormalization. *Phys. Rev. Lett.* **2007**, *99*, 220405.
- [51] Schollwöck, U. The density-matrix renormalization group in the age of matrix product states. *Annals of Physics* **2011**, *326*, 96 – 192, January 2011 Special Issue.
- [52] Verstraete, F.; Nishino, T.; Schollwöck, U.; Bañuls, M. C.; Chan, G. K.; Stoudenmire, M. E. Density matrix renormalization group, 30 years on. *Nature Reviews Physics* **2023**, 1–4.
- [53] Hager, G.; Jeckelmann, E.; Fehske, H.; Wellein, G. Parallelization strategies for density matrix renormalization group algorithms on shared-memory systems. *Journal of Computational Physics* **2004**, *194*, 795 – 808.
- [54] Stoudenmire, E. M.; White, S. R. Real-space parallel density matrix renormalization group. *Phys. Rev. B* **2013**, *87*, 155137.
- [55] Nemes, C.; Barcza, G.; Nagy, Z.; Legeza, Ö.; Szolgay, P. The density matrix renormalization group algorithm on kilo-processor architectures: Implementation and trade-offs. *Computer Physics Communications* **2014**, *185*, 1570 – 1581.
- [56] Milsted, A.; Ganahl, M.; Leichenauer, S.; Hidary, J.; Vidal, G. TensorNetwork on TensorFlow: A spin chain application using tree tensor networks. *arxiv:1905.01331* **2019**,
- [57] Brabec, J.; Brandejs, J.; Kowalski, K.; Xantheas, S.; Legeza, Ö.; Veis, L. Massively parallel quantum chemical density matrix renormalization group method. *Journal of Computational Chemistry* **2021**, *42*, 534–544.
- [58] Zhai, H.; Chan, G. K.-L. Low communication high performance ab initio density matrix renormalization group algorithms. *Journal of Chemical Physics* **2021**, *154*, 0021–9606.
- [59] Gray, J.; Kourtis, S. Hyper-optimized tensor network contraction. *Quantum* **2021**, *5*.
- [60] Unfried, J.; Hauschild, J.; Pollmann, F. Fast time evolution of matrix product states using the QR decomposition. *Phys. Rev. B* **2023**, *107*, 155133.
- [61] Menczer, A.; Legeza, O. Massively Parallel Tensor Network State Algorithms on Hybrid CPU-GPU Based Architectures. *Journal of Chemical Theory and Computation* **2025**, *21*, 1572–1587.
- [62] Menczer, A.; Kapás, K.; Werner, M. A.; Legeza, Ö. Two-dimensional quantum lattice models via mode optimized hybrid CPU-GPU density matrix renormalization group method. *Phys. Rev. B* **2024**, *109*, 195148.
- [63] Menczer, A.; Örs Legeza, Cost optimized ab initio tensor network state methods: industrial perspectives. 2024; <https://arxiv.org/abs/2412.04676>.
- [64] Wilson, K. G. The renormalization group: Critical phenomena and the Kondo problem. *Rev. Mod. Phys.* **1975**, *47*, 773–840.
- [65] White, S. R.; Martin, R. L. Ab initio quantum chemistry using the density matrix renormalization group. *The Journal of Chemical Physics* **1999**, *110*, 4127–4130.
- [66] Legeza, Ö.; Röder, J.; Hess, B. A. QC-DMRG study of the ionic-neutral curve crossing of LiF. *Molecular Physics* **2003**, *101*, 2019–2028.
- [67] Chan, G. K.-L.; Head-Gordon, M. Exact solution (within a triple-zeta, double polarization basis set) of the electronic Schrödinger equation for water. *The Journal of Chemical Physics* **2003**, *118*, 8551–8554.
- [68] Chan, G. K.-L.; Sharma, S. The Density Matrix Renormalization Group in Quantum Chemistry. *Annual Review of Physical Chemistry* **2011**, *62*, 465–481, PMID: 21219144.
- [69] Szalay, Sz.; Pfeffer, M.; Murg, V.; Barcza, G.; Verstraete, F.; Schneider, R.; Legeza, Ö. Tensor product methods and entanglement optimization for ab initio quantum chemistry. *Int. J. Quantum Chem.* **2015**, *115*, 1342–1391.
- [70] Baiardi, A.; Reiher, M. The density matrix renormalization group in chemistry and molecular physics: Recent developments and new challenges. *The Journal of Chemical Physics* **2020**, *152*, 040903.
- [71] Stoudenmire, E.; Schwab, D. J. Supervised Learning with Tensor Networks. *Advances in Neural Information Processing Systems*. 2016.
- [72] Glasser, I.; Sweke, R.; Pancotti, N.; Eisert, J.; Cirac, I. Expressive power of tensor-network factorizations for probabilistic modeling. *Advances in Neural Information Processing Systems*. 2019.
- [73] Glasser, I.; Pancotti, N.; Cirac, J. I. From Probabilistic Graphical Models to Generalized Tensor Networks for Supervised Learning. *IEEE Access* **2020**, *8*, 68169–68182.
- [74] Han, Z.-Y.; Wang, J.; Fan, H.; Wang, L.; Zhang, P. Unsupervised Generative Modeling Using Matrix Product States. *Phys. Rev. X* **2018**, *8*, 031012.
- [75] Puljak, E.; Pierini, M.; Garcia-Saez, A. Tensor Network for Anomaly Detection in the Latent Space of Proton Collision Events at the LHC. *Machine Learning: Science and Technology* **2025**,
- [76] Wang, J.; Roberts, C.; Vidal, G.; Leichenauer, S. Anomaly Detection with Tensor Networks. 2020; <https://arxiv.org/abs/2006.02516>.
- [77] Tomut, A. et al. CompactAI: Extreme Compression of Large Language Models using Quantum-Inspired Tensor Networks. 2024; <https://arxiv.org/abs/2401.14109>.
- [78] Wang, M.; Pan, Y.; Xu, Z.; Li, G.; Yang, X.; Mandic, D.; Cichocki, A. Tensor Networks Meet Neural Networks: A Survey and Future Perspectives. 2025; <https://arxiv.org/abs/2302.09019>.
- [79] Sengupta, R.; Adhikary, S.; Oseledets, I.; Biamonte, J. Tensor networks in machine learning. 2022; <https://arxiv.org/abs/2207.02851>.
- [80] Oseledets, I.; Tyrtshnikov, E. TT-cross approximation for multidimensional arrays. *Linear Algebra and its Applications* **2010**, *432*, 70–88.
- [81] Dolgov, S.; Savostyanov, D. Parallel cross interpolation for high-precision calculation of high-dimensional integrals. *Computer Physics Communications* **2020**, *246*, 106869.
- [82] Gourianov, N.; Lubasch, M.; Dolgov, S.; van den Berg, Q. Y.; Babae, H.; Givi, P.; Kiffner, M.; Jaksch, D. A quantum-inspired approach to exploit turbulence structures. *Nature Computational Science* **2022**, *2*, 30–37, Number: 1 Publisher: Nature Publishing Group.
- [83] Peddinti, R. D.; Pisoni, S.; Marini, A.; Lott, P.; Argenterio, H.; Tiunov, E.; Aolita, L. Quantum-inspired framework for computational fluid dynamics. *Communications Physics* **2024**, *7*, 135, Publisher: Nature Pub-

- lishing Group.
- [84] Gourianov, N.; Givi, P.; Jaksch, D.; Pope, S. B. Tensor networks enable the calculation of turbulence probability distributions. *Science Advances* **2025**, *11*, eads5990.
- [85] Hülst, N.-L. v.; Siegl, P.; Over, P.; Bengoechea, S.; Hashizume, T.; Cecile, M. G.; Rung, T.; Jaksch, D. Quantum-Inspired Tensor-Network Fractional-Step Method for Incompressible Flow in Curvilinear Coordinates. 2025; <http://arxiv.org/abs/2507.05222>, arXiv:2507.05222 [physics].
- [86] White, S. R.; Noack, R. M. Real-space quantum renormalization groups. *Phys. Rev. Lett.* **1992**, *68*, 3487–3490.
- [87] Murg, V.; Verstraete, F.; Legeza, Ö.; Noack, R. M. Simulating strongly correlated quantum systems with tree tensor networks. *Phys. Rev. B* **2010**, *82*, 205105.
- [88] Nakatani, N.; Chan, G. K.-L. Efficient tree tensor network states (TTNS) for quantum chemistry: Generalizations of the density matrix renormalization group algorithm. *The Journal of Chemical Physics* **2013**, *138*, 134113.
- [89] Kurashige, Y.; Saitow, M.; Chalupsky, J.; Yanai, T. Radical O-O coupling reaction in diferrate-mediated water oxidation studied using multireference wave function theory. *Phys. Chem. Chem. Phys.* **2014**, *16*, 11988–11999.
- [90] Kurashige, Y. Multireference electron correlation methods with density matrix renormalisation group reference functions. *Molecular Physics* **2014**, *112*, 1485–1494.
- [91] Murg, V.; Verstraete, F.; Schneider, R.; Nagy, P. R.; Legeza, Ö. Tree Tensor Network State with Variable Tensor Order: An Efficient Multireference Method for Strongly Correlated Systems. *Journal of Chemical Theory and Computation* **2015**, *11*, 1027–1036.
- [92] Larsson, H. R.; Zhai, H.; Gunst, K.; Chan, G. K.-L. Matrix Product States with Large Sites. *Journal of Chemical Theory and Computation* **2022**, *18*, 749–762, PMID: 35060382.
- [93] NVIDIA, NVIDIA Blackwell platform. <https://nvidianews.nvidia.com/news/nvidia-blackwell-platform-arrives-to-power-a-new-era-of-computing>.
- [94] Menczer, A.; Legeza, Ö. Petaflops Density Matrix Renormalization Group Method, unpublished. 2023.
- [95] Dawson, W.; Ozaki, K.; Domke, J.; Nakajima, T. Reducing Numerical Precision Requirements in Quantum Chemistry Calculations. *Journal of Chemical Theory and Computation* **2024**, *20*, 10826–10837, PMID: 39644230.
- [96] McCulloch, I. P.; Gulácsi, M. The non-Abelian density matrix renormalization group algorithm. *Europhysics Letters* **2002**, *57*, 852.
- [97] Tóth, A. I.; Moca, C. P.; Legeza, Ö.; Zaránd, G. Density matrix numerical renormalization group for non-Abelian symmetries. *Phys. Rev. B* **2008**, *78*, 245109.
- [98] White, S. R. Density matrix formulation for quantum renormalization groups. *Phys. Rev. Lett.* **1992**, *69*, 2863–2866.
- [99] Legeza, Ö.; Röder, J.; Hess, B. A. Controlling the accuracy of the density-matrix renormalization-group method: The dynamical block state selection approach. *Phys. Rev. B* **2003**, *67*, 125114.
- [100] Noack, R. M.; Manmana, S. R. Diagonalization- and Numerical Renormalization-Group-Based Methods for Interacting Quantum Systems. *AIP Conference Proceedings* **2005**, *789*, 93–163.
- [101] Dunning, T. H. Gaussian basis sets for use in correlated molecular calculations. I. The atoms boron through neon and hydrogen. *The Journal of Chemical Physics* **1989**, *90*, 1007–1023.
- [102] Chan, G. K.-L.; Kállay, M.; Gauss, J. State-of-the-art density matrix renormalization group and coupled cluster theory studies of the nitrogen binding curve. *The Journal of Chemical Physics* **2004**, *121*, 6110–6116.
- [103] Faulstich, F. M.; Mate, M.; Laestadius, A.; Csirik, M. A.; Veis, L.; Antalík, A.; Brabec, J.; Schneider, R.; Pittner, J.; Kvaal, S.; Legeza, Ö. Numerical and Theoretical Aspects of the DMRG-TCC Method Exemplified by the Nitrogen Dimer. *Journal of Chemical Theory and Computation* **2019**, *15*, 2206–2220.
- [104] Boguslawski, K.; Tecmer, P.; Barcza, G.; Legeza, Ö.; Reiher, M. Orbital Entanglement in Bond-Formation Processes. *Journal of Chemical Theory and Computation* **2013**, *9*, 2959–2973.
- [105] Máté, M.; Petrov, K.; Szalay, S.; Legeza, Ö. Compressing multireference character of wave functions via fermionic mode optimization. *Journal of Mathematical Chemistry* **2023**, *61*, 362–375.
- [106] Goings, J. J.; White, A.; Lee, J.; Tautermann, C. S.; Degroote, M.; Gidney, C.; Shiozaki, T.; Babbush, R.; Rubin, N. C. Reliably assessing the electronic structure of cytochrome P450 on today’s classical computers and tomorrow’s quantum computers. *Proceedings of the National Academy of Sciences* **2022**, *119*.
- [107] Reiher, M.; Wiebe, N.; Svore, K. M.; Wecker, D.; Troyer, M. Elucidating reaction mechanisms on quantum computers. *Proceedings of the National Academy of Sciences* **2017**, *114*, 7555–7560.
- [108] Guthrie, K. et al. NECI: N-Electron Configuration Interaction with an emphasis on state-of-the-art stochastic methods. *The Journal of Chemical Physics* **2020**, *153*, 034107.
- [109] Li, Z.; Li, J.; Dattani, N. S.; Umrigar, C. J.; Chan, G. K.-L. The electronic complexity of the ground-state of the FeMo cofactor of nitrogenase as relevant to quantum simulations. *The Journal of Chemical Physics* **2019**, *150*, 024302.
- [110] Schollwöck, U. The density-matrix renormalization group. *Rev. Mod. Phys.* **2005**, *77*, 259–315.
- [111] In this paper we refer to the use of emulated DGEMM as emulated FP64, even when the number of bits used for emulation is fixed at a level that is insufficient for FP64 accuracy.
- [112] Legeza, Ö.; Sólyom, J. Optimizing the density-matrix renormalization group method using quantum information entropy. *Phys. Rev. B* **2003**, *68*, 195116.
- [113] Legeza, O.; Menczer, A.; Ganyecz, A.; Werner, M. A.; Kapás, K.; Hammond, J.; Xantheas, S. S.; Ganahl, M.; Neese, F. Orbital Optimization of Large Active Spaces via AI-Accelerators. *Journal of Chemical Theory and Computation* **2025**, *21*, 6545–6558.

Supporting Information: In the supporting information we present further numerical results supporting our numerical analysis and conclusions.

In Figs. 6 and 7 we summarize results for systems discussed in Figs. 1 and 2 but obtained on a DGX H100 supercomputer.

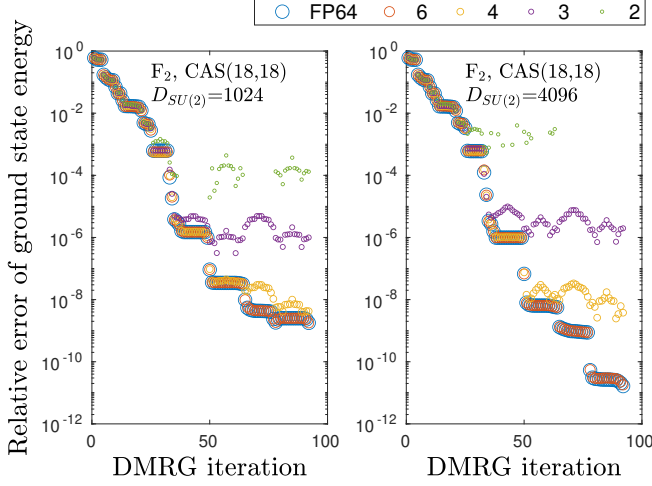


FIG. 6. Similar to Fig. 1 but obtained on a DGX H100 supercomputer.

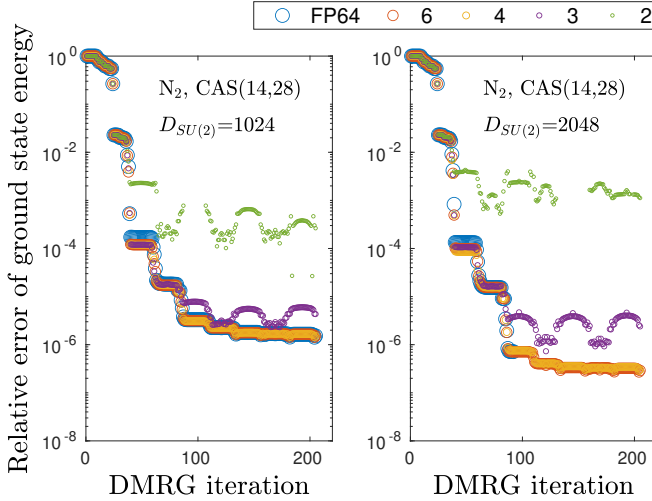


FIG. 7. Similar to Fig. 2 but obtained on a DGX H100 supercomputer.

In Fig. 8 the relative error of the ground state energy, ΔE_{rel} , as a function of DMRG iteration steps is shown for the F_2 molecule in a $\text{CAS}(18,18)$ model space using bond dimension $D_{\text{SU}(2)} = 1024$, $S = 3$ slices, setting the residual error threshold to $\varepsilon = 10^{-5}$ in the Lánczos diagonalization and by switching between CPU and GPU implementations for the renormalization (network contraction) and SVD algorithmic parts. We observe that employing a CPU or GPU based renormalization pro-

cedure, which is mainly based on DGEMM operations,

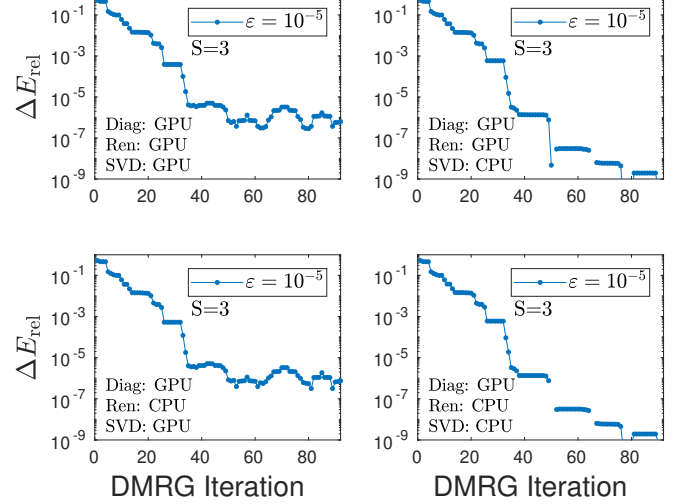


FIG. 8. Relative error of the ground state energy, ΔE_{rel} as a function of DMRG iteration steps for the F_2 molecule in a $\text{CAS}(18,18)$ model space using bond dimension $D_{\text{SU}(2)} = 1024$, $S = 3$ slices, setting the residual error threshold in the Lánczos diagonalization method to $\varepsilon = 10^{-5}$ and employing various CPU and GPU implementations for the renormalization (network contraction) and singular value decomposition (SVD).

has only minor effect on the obtained convergence profile. In contrast to this, switching from the NVIDIA reduced precision cuSOLVER-based GPU implementation of the SVD step (diagonalization of the reduced density matrix) to the CPU variant the accuracy improves significantly. Therefore, the error accumulated via SVD using small number of slices, $S = 3$, determines the overall convergence. Note that similar improvement is achieved by using $S \in \{7, 8\}$ slices or native FP64 in cuSOLVER.

In Fig. 9 the relative error of the ground state energy, ΔE_{rel} , as a function of DMRG iteration steps is shown for the F_2 molecule in a $\text{CAS}(18,18)$ model space using $D_{\text{SU}(2)} = 1024$ and $S = 2$ slices for various residual error threshold values, ε , employed in the Lánczos method. By reducing the residual error, ε , to $10^{-4}, \dots, 10^{-2}$ the number of non-variational eigenvalues disappeared, leading to an oscillating curve in relative energy in the range of 10^{-4} as in Fig. 1 but without “missing” data points.

In Fig. 10 we present similar analysis as shown in Fig. 8 but for $S = 2$ slices. Similarly, as discussed for Fig. 8, employing a CPU or GPU based renormalization procedure has only minor effect on the obtained convergence profile. In contrast to this, switching from the reduced precision cuSOLVER-based GPU implementation of the SVD step (diagonalization of the reduced density matrix) to the CPU variant the accuracy improves significantly. Therefore, as expected, the large error accumulated via SVD using only $S = 2$ slices prohibits DMRG to converge.

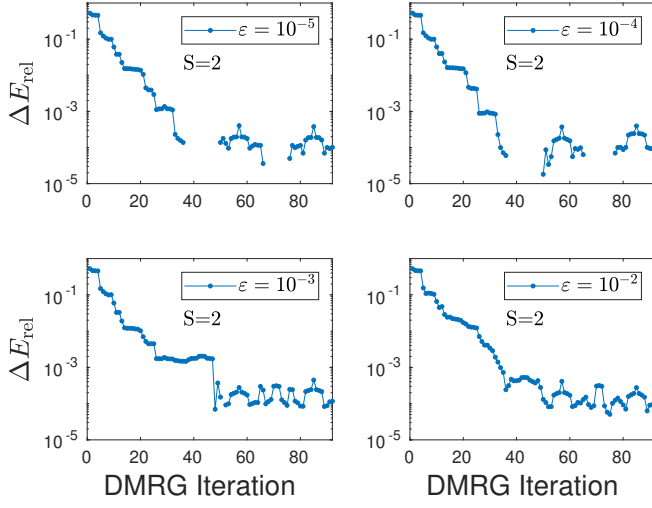


FIG. 9. Relative error of the ground state energy, ΔE_{rel} , as a function of DMRG iteration steps for the F_2 molecule in a CAS(18,18) model space using bond dimension $D_{SU(2)} = 1024$ and $S = 2$ slices for various pre-set residual error threshold values, ε , employed in the Lanczos diagonalization method. Note the missing data points due to non-variational eigenvalues.

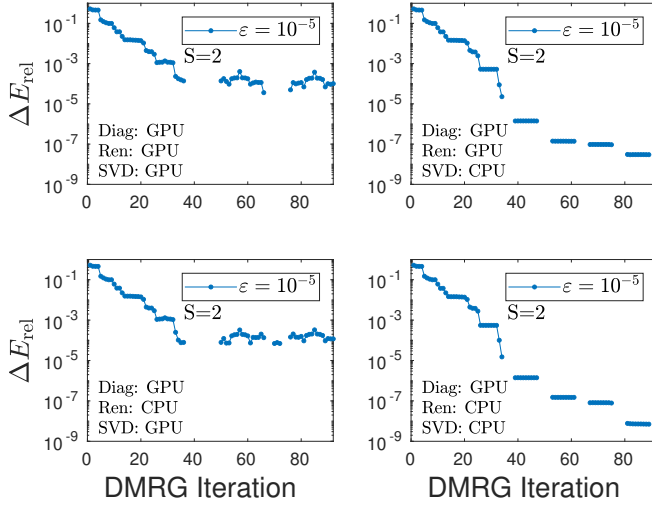


FIG. 10. Similar to Fig 8 but for $S=2$ slices.